Excitations in high-dimensional random-field Ising magnets

Björn Ahrens and Alexander K. Hartmann*
Institute of Physics, University of Oldenburg, 26111 Oldenburg, Germany
(Dated: January 2, 2012)

Domain walls and droplet-like excitation of the random-field Ising magnet are studied in $d = \{3, 4, 5, 6, 7\}$ dimensions by means of exact numerical ground-state calculations. They are obtained using the established mapping to the graph-theoretical maximum-flow problem. This allows to study large system sizes of more than five million spins in exact thermal equilibrium. All simulations are carried out at the critical point for the strength h of the random fields , $h = h_c(d)$, respectively. Using finite-size scaling, energetic and geometric properties like stiffness exponents and fractal dimensions are calculated. Using these results, we test (hyper) scaling relations, which seem to be fulfilled below the upper critical dimension $d_u = 6$. Also, for $d < d_u$, the stiffness exponent can be obtained from the scaling of the ground-state energy.

PACS numbers: 64.60.De, 75.10.Nr, 75.40.-s,75.50.Lk
Keywords: random-field Ising model, stiffness, domain walls, droplets

I. INTRODUCTION

The random-field Ising magnet (RFIM) is one of the most frequently studied models for magnetic systems with quenched disorder. For $d = 3$ and higher dimensions,[1] it is known to undergo a phase transition[2–13] at a critical temperature T_c which depends on the disorder strength. For low temperatures and weak disorder the ferromagnetic interactions dominate and the system is ferromagnetically long-range ordered. For large temperature or strong disorder, the RFIM exhibits no long-range order and behaves like a paramagnet in a field.

Numerically, the nature of this phase transition can be studied in many cases conveniently by means of exact ground-state (GS) calculations (see below), based on an established mapping to the graph-theoretical maximum-flow problem. This allows to treat large system sizes in thermal equilibrium, in contrast to Monte Carlo simulations. For Gaussian disorder, the phase transition is of second order along the full transition line and can be characterized by critical exponents in the usual way, like ν, describing the divergence of the correlation length, and α, describing the behavior of the specific heat. Nevertheless, the RFIM behaves differently compared to the standard ferromagnet. In particular, the hyper-scaling relation $d\nu = 2 - \alpha$ has to be changed[14] by including a positive parameter θ, yielding

$$\nu(d - \theta) = 2 - \alpha\,. \tag{1}$$

In general, the value of θ can be obtained directly from the scaling of domain-wall energies, e.g., induced by changing the boundary conditions, and is known as *stiffness exponent*. The study of such domain-wall excitations was pioneered in the field of spin glasses.[15,16] Here, a comprehensive understanding of the nature of the behavior of two-dimensional spin glasses could be obtained,[17,18] which turned out to be compatible with the droplet picture.[15,19–21]

According the droplet picture, the energy scaling of droplet-like excitations should be the same as for domain walls. For two-dimensional spin glasses, this was recently confirmed via using modified GS algorithms.[22–24] Later on, the value of θ was also determined in higher dimensions[25–29] up to the upper critical dimension, in this case via (heuristic) ground-state calculations before and after changing the boundary conditions, respectively.

For the RFIM, which is the subject of this work, domain-wall studies similar to the spin-glass case, i.e. based on GS calculations, were performed for three- and four dimensions,[7,11] but according our knowledge not in higher dimensions. Droplet type low- or lowest-energy excitations were only obtained in three dimensions so far.[12,30] For three dimensions at finite temperature, also free-energy barrriers where calculated recently.[31,32]

Furthermore, the prediction for the RFIM upper critical dimension $d_u = 6$ was confirmed[13] via exhaustive exact GS calculation up to $d = 7$. This shows that the RFIM can be investigated conveniently by numerical exact algorithms even close to and above the upper critical dimension.

Hence, it is the purpose of this work to study domain-wall and droplet excitations of the RFIM in dimensions $d = 5, 6, 7$ (and for $d = 3, 4$ for comparison), similar to the corresponding $d = 2$ studies for spin glasses, with the striking difference that for the RFIM an exact polynomial-time GS algorithm is available for any dimension, allowing to treat much larger system sizes of more than five million spins in thermal equilibrium. Another difference is that we performed the study for the RFIM right at the zero-temperature disorder-critical point (like the previous work in lower dimensions), since the scaling in the ferromagnetic and paramagnetic phases should be trivial. We analyzed energetic and geometric properties of the excitations using finite-size scaling. We compare the results of different excitations, which should agree according the droplet picture, and verify the above mentioned hyper-scaling relation. Also we compare the geometric (fractal) properties of these excitations. Treating system sizes up to and above the upper critical dimension allows us to observe the transition to mean-field behav-

ior.

To state the model in detail, the RFIM consists of N Ising spins $S_i = \pm 1$ located on the sites of a hyper-cubic lattice with periodic boundary conditions (PBC) in all directions. The spins couple to each other and to local net fields. Its Hamiltonian reads

$$\mathcal{H} = -J \sum_{\langle i,j \rangle} S_i S_j - \sum_i (h\varepsilon_i)\, S_i \,. \qquad (2)$$

It has two contributions. The first covers the spin-spin interaction, where J is the ferromagnetic coupling constant between two adjacent spins and $\langle i, j \rangle$ denotes pairs of next-neighbored spins. The second part of the Hamiltonian describes the coupling to local fields $h_i = h\varepsilon_i$, The factor h is the disorder strength and ε_i the quenched disorder, i.e. Gaussian distributed with zero mean and unit width.

The paper is organized as follows: In section II we describe in principle how the GSs are calculated. The next section covers the definition and use of the different excitations and their theoretical background. Then we state our results in section IV and finish with our conclusions and discussion.

II. GROUND STATES

The phase space of the RFIM consists of a ferromagnetic and a paramagnetic phase. The transition from one phase to the other takes place at a critical point $P_c = (h_c, T_c)$. The transition can be triggered varying the temperature T or varying the standard deviation of the disorder distribution h. From Ref. 33, it is known via renormalization group calculations, that the critical behavior of the RFIM is controlled from the zero-temperature fixed point. Hence, it is possible to focus on $T = 0 =$ const. and vary h to study the phase transition. Here, we concentrated on $T = 0$, $h \approx h_c$, to study excitations right at at the critical point.

At $T = 0$ it is possible to calculate exact ground states in a very efficient way. Following an approach from Ref. 34,35, a d-dimensional hypercubic realization of the disorder $\{h\varepsilon_i\}$ can be mapped to a graph with $N + 2$ nodes and $(d + 2)N + 1$ edges with suitable edge capacities, where N is the number of spins of the RFIM. On this graph a sophisticated maximum flow/minimum cut algorithm can be applied.[36,37] The resulting minimum cut directly correspond to the GS spin configuration $\{S_i\}$ of that specific realization of the disorder. For our simulations the implementation of the maximum flow algorithm from the LEDA library[38] is used. For the RFIM, the actual runtime of the algorithm increases only slightly stronger than linear with the number N of spins.[39]

III. DOMAIN WALLS AND DROPLET EXCITATIONS

We studied two types of excitations, domain walls and droplets.

The domain walls treated in this work separate spin regions which are effected from changed (boundary) conditions from unaffected spins. Following Ref. [7] we forced boundary spins along distinct directions, i.e. up (+) or down (−), at opposite boundaries, respectively. Hence, the PBC are released in that direction, while they are preserved in the remaining $d - 1$ directions. We calculated the GSs for the four possible combinations $+-$, $-+$, $++$, $--$. Three types of spin-regions can be distinguished. The first type can be flipped changing a single boundary condition, i.e. from $++ \rightarrow +-$. We call these spin region *strong controllable*. The second type is just called *controllable*, if it can be flipped by changing both boundary conditions. The third type forms fixed, stable *islands*, unaffected of any boundary-condition change. Examples for regions of such spins are shown in Fig. 1.

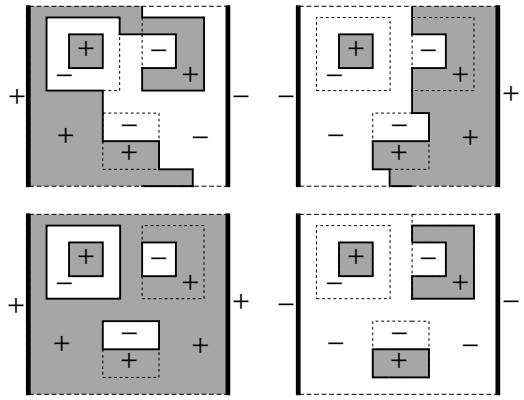

FIG. 1: Fixing the boundary spins (black bars on the left and right of every sketch), forces controllable spins to the direction of the boundary-sign. Areas with $s_i = +1$ are encoded in gray, areas with spins $s_i = -1$ are white. The $d - 1$-dimensional surface between spins of opposite direction is called domain wall (black lines). In some regions, the random fields may freeze the spins into boundary-independent stable islands. Islands may include opposite-directed islands, etc. Hence, islands may also interfere with the domain wall. The dashed lines signal the border of islands within an area of equally-oriented spins, and, at the top and the bottom, the periodic boundary conditions in the remaining $d - 1$ directions.

We also compare two kinds of droplet excitations of the GS. In both cases, the starting point is the GS calculated for full PBC of a realization.

- The first type of excitation is obtained by fixing $(L/3)^d$ spins in the cneter opposite to the their ground-state orientation, respectively. This is inspired by the approach of Ref. 40 for a disordered

solid-on-solid model. This effect can be achieved conveniently by applying strong local fields $\tilde{h}_i$ in the desired direction for the fixed spins. Also, we fixed the spins on hyper-planes of the boundary in parallel to the GS orientation.[20] Note that the spins inside the bulk area create a contribution to the droplet energy via the local fields. To exclude this unwanted effect, we set the local fields ε in the bulk region to zero for the intitial GS calculation. Via a recalculation of the GS of the modified system, this leads to a large excitation with respect to the original realization, not including the boundary, i.e., it is impossible that the fully system flips over. Below, we refer to these excitations as *bulk-induced droplets*, see Fig. 2. From the definition it is clear that these excitations involve $O(L^3)$ spins. Therefore, they come very close to the definition of droplets in the droplet theory[20,21]. To the knowledge of the authors, such droplets have not been studied for the RFIM so far.

- The other type of excitation, called *single-spin-induced droplets*, consists in flipping only the very centered spin and freeze it anti-parallel to its ground-state orientation, again including fixing boundary spins in parallel to the GS. In the same way as for the bulk-induced droplets, this is achieved by applying strong local fields. The droplet created in such a way will include the center spin, but not the boundary. Theses singl-spin-induced droplets will be usually smaller than the bulk-induced droplets. Such excitations have been studied in $d = 3$ so far.[30]

Hence, for each realization $\{h\varepsilon_i\}$ of the disorder, we obtained seven different (ground-state) configurations for diffrt types of boundary conditions/constraints (PBC, $(++)$, $(--)$, $(+-)$, $(-+)$, bulk-induced droplets and single-spin-induced droplets). Technically, to obtain the droplets, we extracted the absolute differences between the spin configuration of two or more GSs via linear combinations of the configurations. Spins with the same properties add to the same value and form connected clusters. These clusters were obtaineded using a breadth-fist-search algorithm. In this way, the calculation of geometric properties of the clusters was very convenient. For the droplets, we measured the domain wall enclosing the droplet, i.e., the droplet surface. In the case of different boundary conditions, we are interested in different definitions of the domain walls, i.e. separating uncontrollable spins vs. controllable spins, strong-controllable spins vs. controllable spins and islands, allowing us to measure different related fractal exponents:

The surfaces are usually not flat or smooth, instead a any type of disorder-averaged surface $A_\circ$ exhibits asymptotically a fractal scaling behavior of the form

$$A_\circ = c_\circ L^{d_\circ}, \tag{3}$$

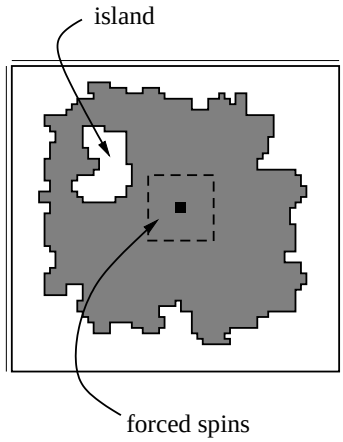

FIG. 2: Spin-wise difference of the pure GS and a droplet is shown. Unchanged spins are shown as white areas ($s_i - s_i' = 0$), changed spins are displayed in gray ($|s_i - s_i'| = 2$).
The excitation is generated, freezing the spins on the boundaries to their pure GS orientation, while the spins on a region in the center are frozen inverted to their ground-state orientation (black dot for the single-spin-induced droplets or dashed square for the bulk-induced droplets). Under these frozen-spin constraints a new GS is calculated. This new configuration is an excitation with respect to the original GS. The resulting droplet may spread to an arbitrary shape with a fractal surface. It also may contain islands.

$d_\circ$ being the corresponding fractal dimension and $c_\circ$ a constant. Dependent on the different boundary and droplet conditions several fractal exponents can be deduced. Partially following the definitions of Ref. [7] we measured

d_s: Surface exponent as dimensionality of the (hyper) surface of unchanged spins within two GSs of $++$ and $+-$ boundary conditions. Technically, we calculate $x_i = |s_i^{++} - s_i^{+-}| = \{0, 2\}$ and count the bonds between the 0-cluster (unchanged spins) and the 2-cluster (changed spins).

d_I: Incongruent interface exponent as dimensionality of the surface of unchanged spins within the three GS of $++$, $+-$ and $--$ boundary conditions. This domain-wall does not include parts of any stable islands. In detail, we calculate $x_i = s_i^{--} + s_i^{++} - 2s_i^{-+} + 4 = \{2, 4, 6\}$. It results to 2 if s_i is strong-controllable. Spins with $x_i = 4$ belong to a stable island and $x_i = 6$, if s_i is just controllable. For the incongruent boundary the bonds only between the 2-cluster and 6-cluster are counted.

d_J: Exchange stiffness exponent, defined as the singed sum of broken bonds, counted positive in the $+-$ and $-+$ configuration and negative for $++$ and $--$.

d_B: fractal exponent of the surface between all flipped and unflipped spins , i.e., number of bonds between

these, for bulk-induced droplets, including islands.

$d_{\rm B}^{(o)}$: same as above, but excluding islands

d_1: fractal exponent of the surface between all flipped and unflipped spins, induced by a single-spin-undiced excitations, including islands.

$d_1^{(o)}$: same as d_1, but excluding islands.

In the case of droplet excitations, we measured additionally the disorder-averaged volume V, i.e., the average number of spins in the cluster of droplet spins

Additionally to the geometric properties of domain walls and droplets we are interested in the stiffness exponent θ, comparing three different types of excitations. The first approach is based on the symmetrized stiffness Σ defined by Middleton and Fisher,[7] i.e., the disorder-averaged symmetrized sum of the boundary-condition dependent energies.

$$\Sigma \equiv \langle E_{+-} + E_{-+} - E_{++} - E_{--} \rangle /2 \,, \tag{4}$$

where E_{pq} is the GS energy for boundary condition $pq \in \{++, --, +-, -+\}$, and $\langle\cdot\rangle$ denotes the disorder average.

A detailed picture of resulting configurations can be found in Fig. 1. Close to criticality, the average stiffness can be assumed to scale as[7]

$$\Sigma(L) \sim L^{\theta} \,. \tag{5}$$

θ denotes the stiffness exponent. According the droplet theory, the energy for other types of excitations of order of system sizes should scale with the same exponent. Hence, for the bulk induced droplets, one should be able to observe

$$\Delta E_{\rm B}(L) \sim L^{\theta} \,, \tag{6}$$

where $\Delta E_{\rm B}$ is the average of the excitation energy of the droplet, i.e., the energy of the droplet configuration for the orginal value of the fields minus the GS energy for the same original values of the fields.

Note that the single-spin-induced droplets tend to be small, i.e., they are not of order of system size. Hence, one cannot directly measure θ from the scaling of the droplet energy. Instead, for the third approach, we followe the arguments of Ref. [30]. Therein, it is shown that the distribution of single-spin-induced droplet radii scales with $p(R) \sim R^{-\theta}$.

IV. RESULTS

We performed exact ground-state calculations for

$d = 3$: $L = 8 \ldots 128$ with $11{\cdot}10^4 \ldots 1{\cdot}10^5$,
$d = 4$: $L = 6 \ldots 45$ with $2{\cdot}10^4 \ldots 2{\cdot}10^5$,
$d = 5$: $L = 6 \ldots 20$ with $2{\cdot}10^3 \ldots 1{\cdot}10^4$,
$d = 6$: $L = 6 \ldots 14$ with $55 \ldots 1{\cdot}10^4$,
$d = 7$: $L = 4 \ldots 8$ with $1{\cdot}10^3 \ldots 1{\cdot}10^4$

d	c_s	d_s	c_J	d_J	c_I	d_I
3	0.90(3)	2.367(9)	5.9(2)	2.178(8)	0.96(3)	2.28(1)
4	0.674(8)	3.924(3)	9.0(2)	3.001(7)	1.261(6)	3.231(2)
5	0.98(2)	4.96(1)	11.7(1)	3.800(4)	1.97(1)	3.925(3)
6	1.37(9)	5.88(3)	16.2(8)	4.56(2)	3.5(2)	4.51(3)
7	1.11(9)	7.06(7)	15(1)	5.57(4)	3.3(3)	5.49(5)

TABLE I: Fit parameters for the scaling of the different surface definitions, i.e. pure surface, Σ_J and the incongruent parts of the domain walls.

realizations of disorder, where the largest size exhibit the smallest number of realizations, respectively. Note that for $d = 4$, we studied $L = 45$ only for the bulk-induced droplets, while we did not included results for bulk-induced droplets in $d > 5$. In general, due to computer main memory restrictions we are limited to system sizes below 5 million spins. We start our analysis with the geometric properties of the domain walls.

A. Domain walls

The surfaces of the three different defined boundary-induced domain walls scale with plain and very clear power laws. Exemplary, the scaling of the simple domain-wall, i.e. $(++)/(+-)$ (yielding the fractal exponent d_s) is shown in Fig. 3. Error bars[41] where obtained as standard error bars from the empirical variance. The other plots look quite the same with the same precision. The scaling exponents d_s, d_J and d_I were found with high *statistical* accuracy. They are stated in Tab. I. Note that the upper limit for any fractal dimension is d, hence the result for d_s at $d = 7$ is an artifact created by the small range of sizes which is accessible at this high dimension. Also, the obtained exponents depend on the fit range, reflecting possible systematic correction to the limiting scaling behavior of Eq. (3). To estimate such systematic errors, we have performed fits for different ranges, leading to the final results which are displayed, c.f. Tab. VII. Given this accuracy, the results for d_J may d_I agree or differ, in particular in large dimensions, see discussion in Sec. V, but d_s differs, comparable to the previously obtained results[7,11] for $d = 3, 4$.

We continue calculating the stiffness exponents. First, the well established ansatz according to Eq. (4) is used for $d = 3, 4, 5, 6, 7$. Our data show well behaved power laws in each dimension, see Fig. 4. The fits of the data points follow Eq. (5), the parameters are stated in Tab. II, in particular the resulting estimate for the stiffness exponentn θ is denoted as $\theta_{\rm dw}$. Varying the ranges of fitted sizes leads to the final estimates, again stated in Tab. VII.

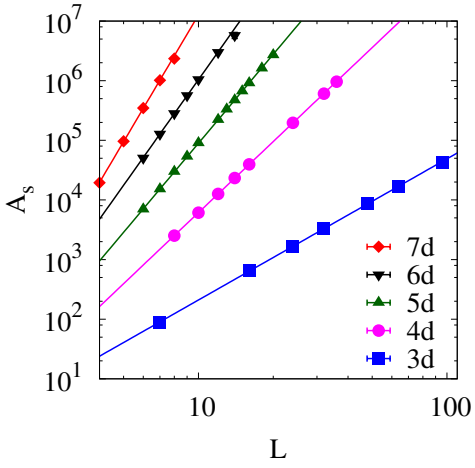

FIG. 3: (color online) Simple surface of domain walls. Most error-bars are smaller than the symbol size. The lines show power-law fits according to Eq. (3).

d	a	$\theta_{\rm dw}$
3	2.42(1)	1.442(2)
4	4.40(3)	1.760(3)
5	7.97(5)	2.146(3)
6	14.6(5)	2.60(1)
7	14.3(6)	3.45(2)

TABLE II: Fit parameters for θ according to Eq. (5)

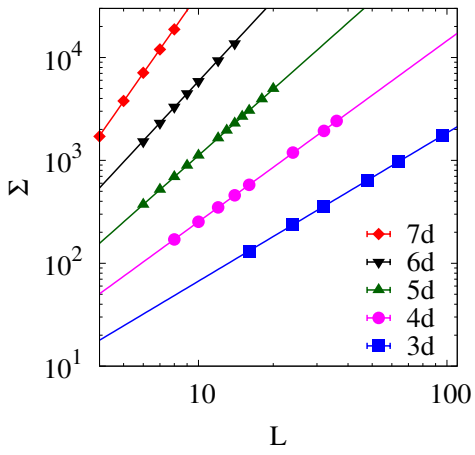

FIG. 4: (color online) Stiffness, as defined in Eq. (4). Most error bars are smaller than the symbol size. Lines display results of fits to power-laws according to Eq. (5).

B. Droplets

Concerning the droplet behavior, we start with the fractal surface properties of the droplets.

We start by using a scatter plot to obtain the relation between surface and volume of single-spin-induced droplets. Theoretically, it should follow a power law of the form

$$A \sim V^{d_1/d}. \tag{7}$$

The fractal surface exponent with and without stable islands can be obtained this way, depending on whether the islands are included in the calculation of A. And indeed, the results exhibit clear power laws, see Fig. 5). Additionally, for each dimension the data points for other system sizes L scatter around the same line, respectively. The fit parameters are listed in Tab. III, for fixed system sizes. The fractal exponents including or ignoring enclosed islands do not differ significantly. We have observed slight changes of the value of d_1 when varying the system size L (unless using very small system sizes where the fitted value of d_1 is much smaller). Hence, the final values we quote, c.f. Tab. VII, are slightly different and involve larger error bars than the pure statistical error bars. When approaching large dimensions d_s gets close to the dimension of the system, in particular right at the upper critical dimension. The result for the fractal dimensions is, given the unknown correlations to scaling, in fair agreement with the results for d_s as shown in Tab. I.

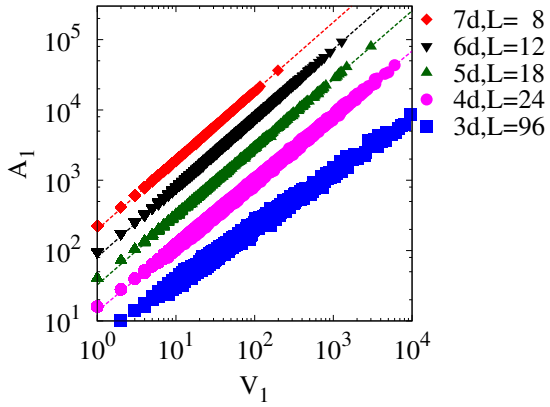

FIG. 5: (color online) Scatter plot of the enclosing surface, i.e., not counting islands inside the droplet, of single-spin-induced droplets as function of their volume. The surface is scaled up with a factor of $k = 1, 2, 4, 8, 16$ for $d = 3, 4, 5, 6, 7$ to separate the data visually.

The bulk-induced droplets have the disadvantage that a smaller effective range of sizes if accessible: The minimal system size to generate such a droplet excitation must be $L = 6$. In linear direction, one spin is used to fix the boundary and at least another one is needed at the very center to form the "large core". Though, only two spin in each direction are left to form the droplet. In the

d	c_1	d_1	$c_1^{(o)}$	$d_1^{(o)}$
3	6.07(2)	2.32(1)	6.02(2)	2.33(1)
4	6.88(1)	3.70(1)	6.87(1)	3.70(1)
5	8.15(3)	4.87(1)	8.51(2)	4.87(1)
6	10.13(1)	5.91(1)	10.13(1)	5.91(1)
7	12.49(3)	6.88(1)	12.53(3)	6.86(1)

TABLE III: Fit parameters for the scaling of the enclosing surface and ragged surface for single-spin-induced droplets, calculated in a large system size with high sample number, system sizes as in Fig. 5.

d	c_B	d_B	$c_B^{(o)}$	$d_B^{(o)}$
3	4.300(4)	2.3282(2)	2.761(3)	2.660(2)
4	4.085(3)	3.7257(2)	4.024(3)	3.7328(2)
5	6.10(3)	4.758(2)	6.10(3)	4.758(2)

TABLE IV: Fit parameters for the scaling of the enclosing surface and ragged surface for bulk-induced droplets. For $d > 4$, data is not available in high quality for large-enough system sizes.

same way, also for larger sizes, the volume accessible for the droplets to form is smaller, leading to stronger finite-size corrections, see below. This means, for $d > 5$ the range of system sizes ($L \geq 6$) is too small to observe the leading scaling behavior. Hence, we restrict our analysis for the bulk-induced droplets to $d = 3, 4$ and $d = 5$.

In Fig. 6 a scatter-plot of the enclosing surface as function of the volume can be seen. For the fits the ansatz according Eq. (7) was made, but using d_B instead of d_1. From the large number of data points the fit parameters can be obtained, by using the data points for all system sizs in one fit, with high statistical accuracy. The fit parameters can be found in Tab. IV. Given the small ranges of system sizes here and unknown corrections to scaling, the agreement with the results for the single-spin-induced droplets is fair.

Systematic finite-size corrections are negelected by this single fit of the scatter-plot data. Hence, to estimate these corrections, leading to the results stated in Tab. VII, we proceeded as follows: Instead of observing the scatter-plot, the mean of the enclosing surface can be analyzed as function of the system size. A power law as $A_B(L) = c_B(L - L_0)^{d_B}$ leads to the best fits. The length-scale correction L_0 covers finite-size effects. Of course, an ansatz using a correction term $c_B L^{d_B}(1 + c_2 L^{d'})$ can be used too, but the correction term involves one more parameter. Anyway, fitting $A_B(L)$, leads to similar exponents compared to those as obtained from the scatter plot, see Tab. V. Again, the results for the different approaches for surface measurement do not lead to significantly different results.

Next, we discuss energetic properties of droplets, aiming at estimating the stiffness exponent θ.

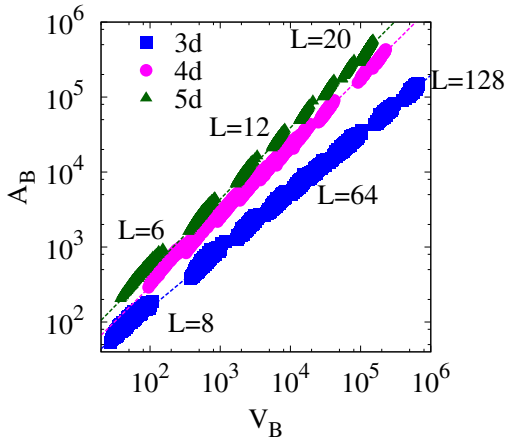

FIG. 6: (color online) Scatter plot of the enclosing surface of bulk-induced droplets as function of their volume for $d = 3, 4, 5$. The lower right labels show system sizes of the $3d$ data, the upper left show those for $5d$. $4d$ is unlabeled.

d	c_B	L_0	d_B	$c_B^{(o)}$	$L_0^{(o)}$	$d_B^{(o)}$
3	1.37(8)	2.2(1)	2.35(2)	1.02(6)	1.88(9)	2.44(1)
4	0.49(5)	1.50(9)	3.79(3)	0.48(5)	1.49(9)	3.80(3)
5	0.8(2)	2.0(1)	4.54(6)	0.8(2)	2.0(1)	4.54(6)

TABLE V: Fit parameters for the scaling of the enclosing surface and ragged surface for bulk-induced droplets when scaling the surface as a function of system size. For $d = 6, 7$, a large-enough range of system sizes is not available.

The singe-spin droplets are known to tend to be very small.[30] This property prohibits the direct measurement of the stiffness exponents from the relation of droplet energy to linear droplet size. Nevertheless, the distribution of droplet radii R follows[30] approximately a power law $P(R) \sim R^{-\theta}$, when the data is binned logarithmically. Hence, we obtained the distribution of droplet radii. For $d = 3, 4, 5$ a logarithmic binning of the data points is possible. For larger dimensions, the achievable systems sizes seem to be too small to get a histogram of sufficient statistical quality. The histograms can be seen in Fig. 7. There exist regions in which the radii distribution follows $R^{-\theta}$, when using the values $\theta_{\rm dw}$ obtained from the domain-wall measurements. This confirms somehow the results of Ref.[30] for higher dimensions $d = 4, 5$. Nevertheless, the distribution itself is not sufficient to determine the stiffness in a meaningful way if the value of θ was not known from other sources.

For the bulk-induced droplets, their length scale is fixed to be $O(L)$, as assumed in the droplet theory[20,21]. Hence, one could hope that the scaling of the droplet energy is governed by the (stiffness) exponent θ. We looked at the scaling of the difference between the GS energies

of the original system and the GS for the bulk-induced droplets (calculated with the original set of random fields, respectively). The resulting average bulk droplet energies $\Delta E_{\rm B}$ are shown in Fig. 8 for $d = 3, 4$. A clear curvature is visible, hence strong finite-size corrections to Eq. (6). This can be explained by the fact that, due to the extensive size of the bulk area, the effective volume which is accessible for the droplet to arrange is much smaller. In particular this means, that for higher dimension $d > 4$ the linear sizes L which are accessible are to small to come even just near to the final scaling behavior. Hence, we have restricted ourself for the energetic properties of the bulk-induced droplets to dimensions $d = 3$ and 4. To include corrections to scaling, we fitted the data can by using

$$\Delta E_B = a(L - L_0)^{\theta_{\rm B}} \,, \tag{8}$$

see Tab. VI. The minimum system size $L_{\rm min}$ included in the fit was chosen such that the fitting quality (measured by the weighted sum of square residuals per degree of freedeom, denoted as `WSSER/ndf` in `gunplot`) was acceptable, i.e., around 1. To furthermore estimate systematic corrections, we also performed fits for larger values of $L_{\rm min}$, respectively, leading to the final results for $\theta_{\rm B}$ as stated in Tab. VII. Within error bars, the values for the droplet stiffness are compatible with the results obtained for the domain walls. Hence, it appears that indeed the basic assumptions of the droplet theory is true that different types of excitations are universally described by the same exponents.

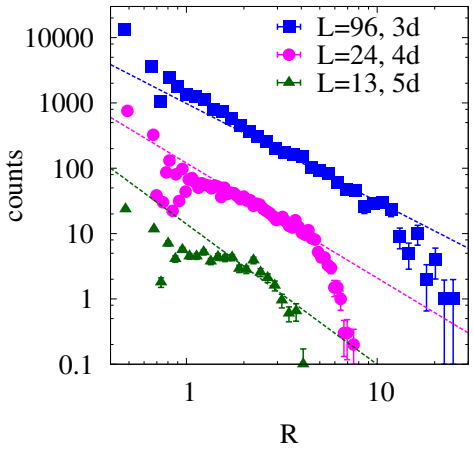

FIG. 7: (color online) Number of single-spin-induced droplets with a radius in a specific interval for $d = 3$, $L = 96$, $d = 4$, $L = 24$ and $d = 4$, $L = 13$. The latter down scaled by a factor 10 and 20, respectively. The lines are power laws using the stiffness exponents.

d	$L_{\rm min}$	a	L_0	$\theta_{\rm B}$
3	15	5.34(15)	2.42(10)	1.501 (7)
4	12	7.41(18)	2.75 (5)	1.91 (1)

TABLE VI: Fit parameters for the scaling of the droplet energy according to Eq. (8). The fits were performed for a range of system sizes rangeing from $L_{\rm min}$ to the largest system sizes considered here, respectively.

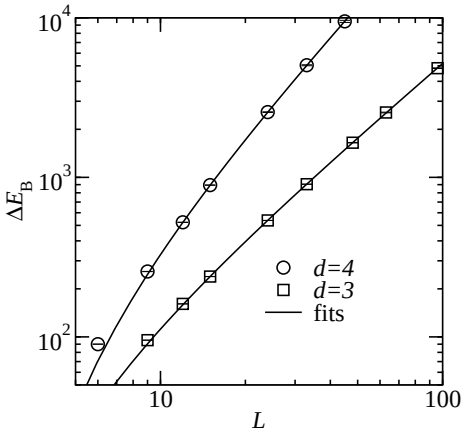

FIG. 8: Scaling of the excitation energy $\Delta E_{\rm B}$ of bulk-induced droplets for $d = 3$ and $d = 4$. Lines show fits to power-laws $\Delta E_B \sim (L - L_0)^{\theta}$, with $\theta = 1.50$ (3d) and $\theta = 1.91$ (4d).

C. Scaling of ground-state energy

There seems to exist a third alternative way of determining the stiffness exponent, not related to externally induced domain walls and droplets. For spin glasses in finite and low dimensions with PBC, it has been conjectured[42] and numerically observed for two dimensions[43] that the finite-size behavior of the (total) GS energy E_L of the unperturbed system is given by

$$E_L = E_\infty + aL^{\theta} \,. \tag{9}$$

The explanation is that the PBC induce "hidden" domain walls (with respect to free boundary conditions), which dominate the finite-size corrections above higher order contributions. Hence, we have reanalyzed the data of previous work.[6,10,13] The results of θ from fitting (9) to the GS energies can be found in Fig. 9, its exponents are listed as $\theta_{\rm E}$ in Tab. VII. Comparing with the results for the stiffness exponent $\theta_{\rm dw}$, the assumptions seems to be indeed true for $d < d_u = 6$, maybe also at $d = d_u$ (given that we state here only statistical error bars, hence true error bars are likely larger). The assumption of Eq. (9) is certainly not true above the upper critical dimension. It seems rather that the exponent for GS energy finite-size correction attains some mean-field value for $d \geq d_u$. Interestingly, $\theta_{\rm E}$ agrees within error bars with γ/ν in all dimensions $d = 3, \ldots, 7$.

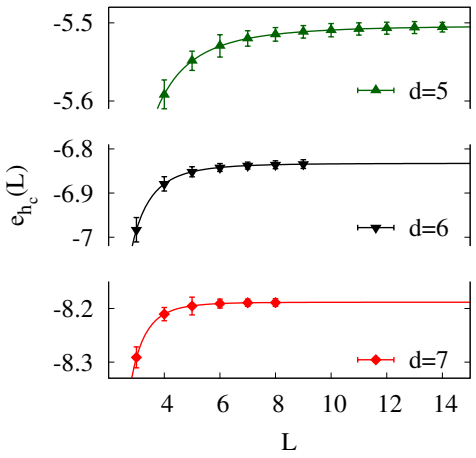

FIG. 9: (color online) Scaling of the ground-state energy at the critical point. The lines show fits to Eq. (9).

	$d=3$	$d=4$	$d=5$	$d=6$	$d=7$
h_c	2.28(1)	4.18(1)	6.02(2)	7.78(1)	9.48(3)
β	0.017(5)	0.13(5)	0.25(1)	0.50(5)	0.50(5)
γ	1.98(7)	1.57(10)	1.3(1)	1.07(5)	1.0(2)
α	0	0	0	0	0
ν	1.37(9)	0.78(10)	0.60(3)	0.50(5)	0.47(5)
$\tilde{\theta}=\gamma/\nu$	1.4(2)	2.0(4)	2.3(3)	2.1(5)	2.2(5)
θ_{E}	1.49(3)	1.81(6)	2.03(2)	2.42(2)	2.42(2)
θ_{dw}	1.44(2)	1.75(2)	2.15(1)	2.60(2)	3.5(1)
d_J-1/ν	1.4(1)	1.65(15)	2.1(1)	2.5(2)	3.5(1)
θ_{B}	1.51(2)	1.8(1)	—	—	—
d_s	2.37(2)	3.92(6)	4.9(2)	5.8(8)	6.9(2)
d_1	2.32(1)	3.73(10)	4.9(1)	5.9(1)	6.9(1)
d_B	2.35(2)	3.79(4)	4.6(1)	—	—
d_J	2.14(3)	2.93(2)	3.79(2)	4.54(2)	5.5(1)
d_I	2.25(2)	3.23(1)	3.92(1)	4.5(2)	5.4(2)

TABLE VII: Previous results[7,11,13] above the big line and new, final results below. The upper half of the final results contains different estimates for the stiffness exponent, while the bottom part contains measured for the fractal properties of domain walls. Note that the values stated here differ usually from the values given in the lists of fit parameters since they the former include systematical errors, which were estimated by varying the range of fitted system sizes and observing the change of the resulting parameters.

V. CONCLUSION AND DISCUSSION

To calculate ground states of the RFIM numerically, we applied a well-known mapping to the maximum-flow problem. Using efficient polynomial-time-running maximum-flow/minimum-cut algorithms, we were able to study large systems sizes up to 5×10^6 spins in exact equilibrium at $T = 0$.

Comparing the GS configurations obtained from different constraints leads to suitably defined domain-wall and droplet excitations. We obtained fractal surface exponents and the stiffness exponent in $d = 3, 4, 5, 6, 7$ for these excitations, see final results in Tab. VII. The values for domain walls stated in the literature[7,11] for $d = 3, 4$ could be recovered. For all dimensions, different types of excitations are described, within error bars, by the same value of the stiffness exponents, as assumed by the droplet theory.[20,21] In particular, (bulk) droplet excitations have been calculated for the RFIM for the first time and found to be compatible with domain walls. Also, the result for θ_{dw} is according a scaling relation[7] equal to $d_J - 1/\nu$, which is fulfilled within error bars for all dimensions. Furthermore, the scaling inequality[44,45] $d/2 - \beta/\nu \leq \theta \leq \theta/2$ is fullfilled in all dimensions.

On the other hand, the hyperscaling relation (1) is fulfilled within error bars only for $d = 3, 4, 5$, but not for $d = 6, 7$. Usually, hyper-scaling relations, involving the dimension d, are not valid im the mean-field regime, i.e., above the upper critical dimension. Nevertheless, motivated by our results for $d = 7$, it is compatible with the data if we change the hyperscaling relation in the following way: We know from earlier work in high dimensions that above the upper critical dimension d_u when performing a data collapse, a rescaling of the linear system size according to $L \to L^{d/d_u}$ has to be performed.[46] Since the length rescaling enters into scaling relations via the correlation length[47,48] $\xi_L/L \sim \tilde{\xi}(L^{1/\nu}(h - h_c))$, the correlation length exponent ν needs to be replaced with $\nu^* = \nu_{\mathrm{MF}} d_u/d$ when performing a data collaps. If we transfer this change to the hyper-scaling relation, it reads $\theta = d - (2 - \alpha)/\nu^*$. Inserting in $d = 7$, $d_u = 6$, $\alpha = 0$ and $\nu_{\mathrm{MF}} = 0.5$, this leads to $\theta^{(7)} = 3.5$ without any further assumptions. This matches very well to $\theta^{(7)} = 3.5(1)$ as found in this study. On the other hand, a simple rescaling in $d = 6$ appears not possible to us, since a replacement $L \to L \ln^{1/6} L$ was found previously,[13] so rescaled exponents can not be obtained in a simple way, hence a different kind of hyperscaling seems to be necessary here.

Also the fractal properties of the droplets and domain walls found for lower dimensions extent to larger dimensions. In particular, the "geometrically" measured values d_s, d_1 and d_{B} agree for all dimensions within error bars. Finally, the values for d_I and d_J, measuring different fractal properties of the domain walls, may or may not be equivalent, as already discussed in previously[7,11] for the cases $d = 3$ and $d = 4$, were also a possible scaling relation $d_I = d_J + \beta/\nu$ was presented. For $d \geq 6$ this relation is clearly not fullfiled here, which may be also due to the failing of hyperscaling at and above the upper critical dimension.

VI. ACKNOWLEDGMENTS

We thank K. Binder, S. Boettcher, A. Hucht, O. Melchert, M. Mézard, U. Nowak, H. Rieger, D. Sherrington, and D. Stauffer for useful discussions. The calculations were carried out on **GOLEM** (**G**roßrechner **OL**denburg für **E**xplizit **M**ultidisziplinäre **F**orschung)

and the **HERO** (**H**igh-**E**nd Computing **R**esource **O**ldenburg) at the University of Oldenburg.

---

* Electronic address: a.hartmann@uni-oldenburg.de

[1] J. Bricmont and A. Kupiainen, Phys. Rev. Lett. **59**, 1829 (1987).
[2] M. Gofman, J. Adler, A. Aharony, A. B. Harris, and M. Schwartz, Phys. Rev. Lett. **71**, 1569 (1993).
[3] H. Rieger, Phys. Rev. B **52**, 6659 (1995).
[4] U. Nowak, K. D. Usadel, and J. Esser, Physica A: Statistical and Theoretical Physics **250**, 1 (1998).
[5] A. K. Hartmann and U. Nowak, Eur. Phys. J. B **7**, 105 (1999).
[6] A. K. Hartmann and A. P. Young, Phys. Rev. B **64**, 214419 (2001).
[7] A. A. Middleton and D. S. Fisher, Phys. Rev. B **65**, 134411 (2002).
[8] C. Frontera and E. Vives, Computer Physics Communications **147**, 455 (2002).
[9] E. T. Seppälä, A. M. Pulkkinen, and M. J. Alava, Phys. Rev. B **66**, 144403 (2002).
[10] A. K. Hartmann, Phys. Rev. B **65**, 174427 (2002).
[11] A. A. Middleton, preprint arXiv:cond-mat/0208182 (2002).
[12] M. Zumsande, M. J. Alava, and A. K. Hartmann, J. Stat. Mech. p. P02012 (2008).
[13] B. Ahrens and A. K. Hartmann, Phys. Rev. B **83**, 014205 (2011).
[14] G. Grinstein, Phys. Rev. Lett. **37**, 944 (1976).
[15] W. L. McMillan, J. Phys. C **17**, 3179 (1984).
[16] A. J. Bray and M. A. Moore, J. Phys. C **17** (1984).
[17] A. K. Hartmann and A. P. Young, Phys. Rev B **64**, 180404 (2001).
[18] A. K. Hartmann, A. J. Bray, A. C. Carter, M. A. Moore, and A. P. Young, Phys. Rev. B **66**, 224401 (2002).
[19] A. J. Bray and M. A. Moore, in *Heidelberg Colloquium on Glassy Dynamics*, edited by J. L. van Hemmen and I. Morgenstern (Springer, Berlin, 1987), p. 121.
[20] D. S. Fisher and D. A. Huse, Phys. Rev. Lett. **56**, 1601 (1986), URL http://link.aps.org/doi/10.1103/PhysRevLett.56.1601.
[21] D. S. Fisher and D. A. Huse, Phys. Rev. B **38**, 386 (1988).
[22] A. K. Hartmann and M. A. Moore, Phys. Rev. Lett. **90**, 127201 (2003).
[23] A. K. Hartmann and M. A. Moore, Phys. Rev. B **69**, 104409 (2004).
[24] A. K. Hartmann, Phys. Rev. B **77**, 144418 (2008).
[25] A. K. Hartmann, Phys. Rev. E **59**, 84 (1999).
[26] A. K. Hartmann, Phys. Rev. E **60**, 5135 (1999).
[27] S. Boettcher, Eur. Phys. J. B **38**, 83 (2004), ISSN 1434-6028, 10.1140/epjb/e2004-00102-5, URL http://dx.doi.org/10.1140/epjb/e2004-00102-5.
[28] S. Boettcher and A. K. Hartmann, Phys. Rev. B **72**, 014429 (2005).
[29] S. Boettcher, Phys. Rev. Lett. **95**, 197205 (2005).
[30] Zumsande, M. and Hartmann, A. K., Eur. Phys. J. B **72**, 619 (2009), URL http://dx.doi.org/10.1140/epjb/e2009-00410-2.
[31] N. G. Fytas, A. Malakis, and K. Eftaxias, Journal of Statistical Mechanics: Theory and Experiment **2008**, P03015 (2008), URL http://stacks.iop.org/1742-5468/2008/i=03/a=P03015.
[32] R. L. C. Vink, T. Fischer, and K. Binder, Phys. Rev. E **82**, 051134 (2010), URL http://link.aps.org/doi/10.1103/PhysRevE.82.051134.
[33] A. J. Bray and M. A. Moore, J. Phys. C: Solid State Phys. **18**, 927 (1985).
[34] J. C. Picard and H. D. Ratliff, Networks **5**, 357 (1975).
[35] A. T. Ogielski, Phys. Rev. Lett. **57**, 1251 (1986).
[36] A. V. Goldberg and R. E. Tarjan, J. ACM **35**, 921 (1988), ISSN 0004-5411.
[37] A. K. Hartmann and H. Rieger, *Optimization Algorithms in Physics* (Wiley-VCH, Berlin, 2001), ISBN 978-3-527-40307-3.
[38] K. Mehlhorn and S. Näher, *The LEDA Platform of Combinatorial and Geometric Computing* (Cambridge University Press, Cambridge, 1999), URL http://www.algorithmic-solutions.de.
[39] A. A. Middleton, Phys. Rev. Lett. **88**, 017202 (2001), URL http://link.aps.org/doi/10.1103/PhysRevLett.88.017202.
[40] K. Schwarz, A. Karrenbauer, G. Schehr, and H. Rieger, Journal of Statistical Mechanics: Theory and Experiment **2009**, P08022 (2009), URL http://stacks.iop.org/1742-5468/2009/i=08/a=P08022.
[41] A. K. Hartmann, *A Practical Guide To Computer Simulation* (World Scientific Publishing Company, 2009), ISBN 978-9812834157.
[42] J.-P. Bouchaud, F. Krzakala, and O. C. Martin, Phys. Rev. B **68**, 224404 (2003).
[43] I. A. Campbell, A. K. Hartmann, and H. G. Katzgraber, Phys. Rev. B **70**, 054429 (2004).
[44] D. S. Fisher, Phys. Rev. Lett. **56**, 416 (1986).
[45] M. Schwartz and A. Soffer, Phys. Rev. Lett. **55**, 2499 (1985).
[46] J. L. Jones and A. P. Young, Phys. Rev. B **71**, 174438 (2005).
[47] V. E. Privman, *Finite Size Scaling and Numerical Simulation of Statistical Systems* (World Scientific Publishing Company, 1990), ISBN 978-9810237967.
[48] E. Brézin, J. Phys. France **43**, 15 (1982).